



Photocatalytic degradation of ketorolac tromethamine (KTC) using Ag-doped ZnO microplates

Amandeep Kaur¹, Alex O. Ibhaddon², and Sushil Kumar Kansal^{1,*}

¹Dr. S.S. B. University Institute of Chemical Engineering and Technology, Panjab University, Chandigarh, India

²Department of Chemical Engineering, School of Engineering, University of Hull, Cottingham Road, Hull HU6 7RX, UK

Received: 21 November 2016

Accepted: 6 January 2017

Published online:

16 January 2017

© Springer Science+Business Media New York 2017

ABSTRACT

In this study, Ag-doped ZnO microplates were prepared via precipitation technique and further characterized by FESEM, EDS, XRD, FTIR, TGA, XPS, UV-DRS and RT-PL techniques. The outcomes indicated that Ag⁺ ions were well incorporated into ZnO lattice leading to the absorption of ZnO in visible region as well as effective charge separation. The photocatalytic experiments exhibited that Ag-doped ZnO microplates show higher catalytic activity (91%) than bare ZnO (71%) for the degradation of KTC drug under solar illumination. The photocatalytic degradation of KTC drug over Ag-doped ZnO microplates obeyed pseudo first-order kinetics model. Also, the role of active species was examined by the addition of several scavengers in the photocatalytic degradation system. The results indicated that h⁺, OH_s, ¹O₂ and OH were considered as prime reactive species in photocatalytic degradation process.

Introduction

In recent years, researchers have put significant efforts in developing methods to utilize solar energy more effectively in order to provide solution to one of the world's major problem, energy crisis. One promising approach is to synthesize highly active photocatalysts to promote the water splitting, photocatalytic treatment of environment pollutants, or both under solar illumination [1–3]. Among various materials, metal oxide-based nanostructures have gained considerable attention owing to their high surface to volume ratio, adjustable band gap and high stability [4–7]. ZnO has been regarded as a promising catalyst because of its low cost, non-toxic

nature and high electron stability [8–11]. But it can only be activated under UV light because of the band gap (i.e. 3.2 eV) and electron–hole recombination; thereby, its photocatalytic efficiency is low because of limited adsorption of solar light [12]. Therefore, recent research has been focused to design ZnO-based photocatalysts with longer wavelength capability for light absorption in the full solar spectrum [13].

In order to achieve broad wavelength spectrum for ZnO, two common approaches are used—doping with metals (Ag, Au, Pt, etc.), non-metals (carbon, nitrogen, sulphur, etc.) and composites with lower band gap semiconductors such as CuO, CdS, Fe₂O₃, and CdSe [14–18]. Among these methods, band gap

Address correspondence to E-mail: sushilkk1@yahoo.co.in; sushilkk1@pu.ac.in

modification of ZnO through metal doping is considered as one of the most effective approach to extend the absorption of light into visible region by suppressing electron–hole recombination. It was confirmed that doping with small concentrations increases the lifespan of photogenerated charge carriers and thereby, improved photocatalytic degradation efficiency [19, 20]. Recent studies have shown that silver is the best doping element because of its larger ionic size, least orbital energy and high solubility [21]. It should be noted that not all transition metals give a positive response. In some cases, transition metals reduce the photocatalytic degradation efficiency because of increase in electron–hole recombination.

Herein, we report a precipitation method for preparing Ag-doped ZnO photocatalyst. The as-prepared materials were further characterized using a suite of spectroscopic, microscopic, thermal and other techniques to examine their compositional, morphological, optical and luminescent behaviour. The activity of the photocatalyst prepared was studied in the degradation of a biorecalcitrant organic pollutant, ketorolac tromethamine (KTC) under solar irradiation. Also, the impact of pH and catalyst loading on degradation efficiency was examined.

Experimental section

Materials and methods

Zinc acetate dehydrate ($\geq 98\%$ purity), silver nitrate ($\geq 99\%$ purity), sodium hydroxide ($>97\%$ purity), sodium azide ($\geq 99.5\%$ purity), sodium chloride ($\geq 99\%$ purity) and potassium iodide ($\geq 99\%$ purity) were procured from Merck, India. Isopropanol (99% purity) was obtained from SD Fine Chem Limited, India. Ketorolac tromethamine (KTC) was provided by Saurav Chemicals Limited, Derabassi, India. Double distilled water (DDW) was utilized to brew all stock solutions, and reagents were used as received. 0.1 N solutions of HCl and NaOH were added to regulate the pH of KTC solution with Mettler Toledo pH-meter.

Ag-doped ZnO photocatalyst was synthesized using similar precipitation method as reported earlier [22]. To synthesize Ag-doped ZnO, firstly, 0.05 mol of zinc acetate dihydrate was mixed in 50 mL double

distilled water. Subsequently, 1 M NaOH aqueous solution was added dropwise to achieve the pH of the suspension to about pH 12. After that, 0.025% of AgNO₃ was dissolved in ethanol–water mixture (1:1) and then added dropwise into the solution and stirred for 16 h. The obtained precipitates were washed thoroughly with ethanol and then with DDW, filtered and finally dried in an oven at 80 °C for overnight. Pure ZnO was also obtained using same procedure except adding up AgNO₃ salt.

Characterization

The morphology of the catalyst prepared was examined using field emission scanning electron microscope (Hitachi-8010). The structure and crystallinity of synthesized samples were examined on powder X-ray diffraction (PXRD) instrument. The scan analysis was operated within 2θ range of 10°–80° by Cu $K\alpha$ radiation. Fourier transform infrared (FTIR) spectra of samples were obtained from Thermofisher Nicolet iS50 spectrometer in the range of 400–4000 cm⁻¹. TGA analysis was conducted on PerkinElmer STA 6000 instrument using nitrogen gas with a heating rate of 10 °C per min. The chemical composition and electronic states of samples were scrutinized on X-ray photoelectron spectroscopy (XPS) with monochromated Mg $K\alpha$ X-ray ($h\nu = 1253.6$ eV) radiation. UV–Vis diffuse reflectance (DRS) of samples was carried out on UV–Vis (Shimadzu, UV-2600) spectrophotometer using BaSO₄ as reference. Room temperature photoluminescence (RT-PL) spectra of samples were obtained using fluorescence spectrophotometer (Hitachi F-7000) at an excitation wavelength of 340 nm.

Photocatalytic experiments

The photocatalytic activity of Ag-doped ZnO was tested by degrading the KTC under solar light irradiation (65–70 K lux, recorded on CHY 332 light meter). In a photocatalytic experiment, 0.25 g of as-synthesized photocatalyst was dispersed into 100 mL of aqueous solution of KTC drug. Adsorption–desorption equilibrium is accomplished in 30 min in dark prior to light illumination to initiate the degradation reaction. Then, 2 mL aliquot was extracted at specific time periods and filtered through 0.45- μm Chromafil syringe filter. The absorbance of filtrate

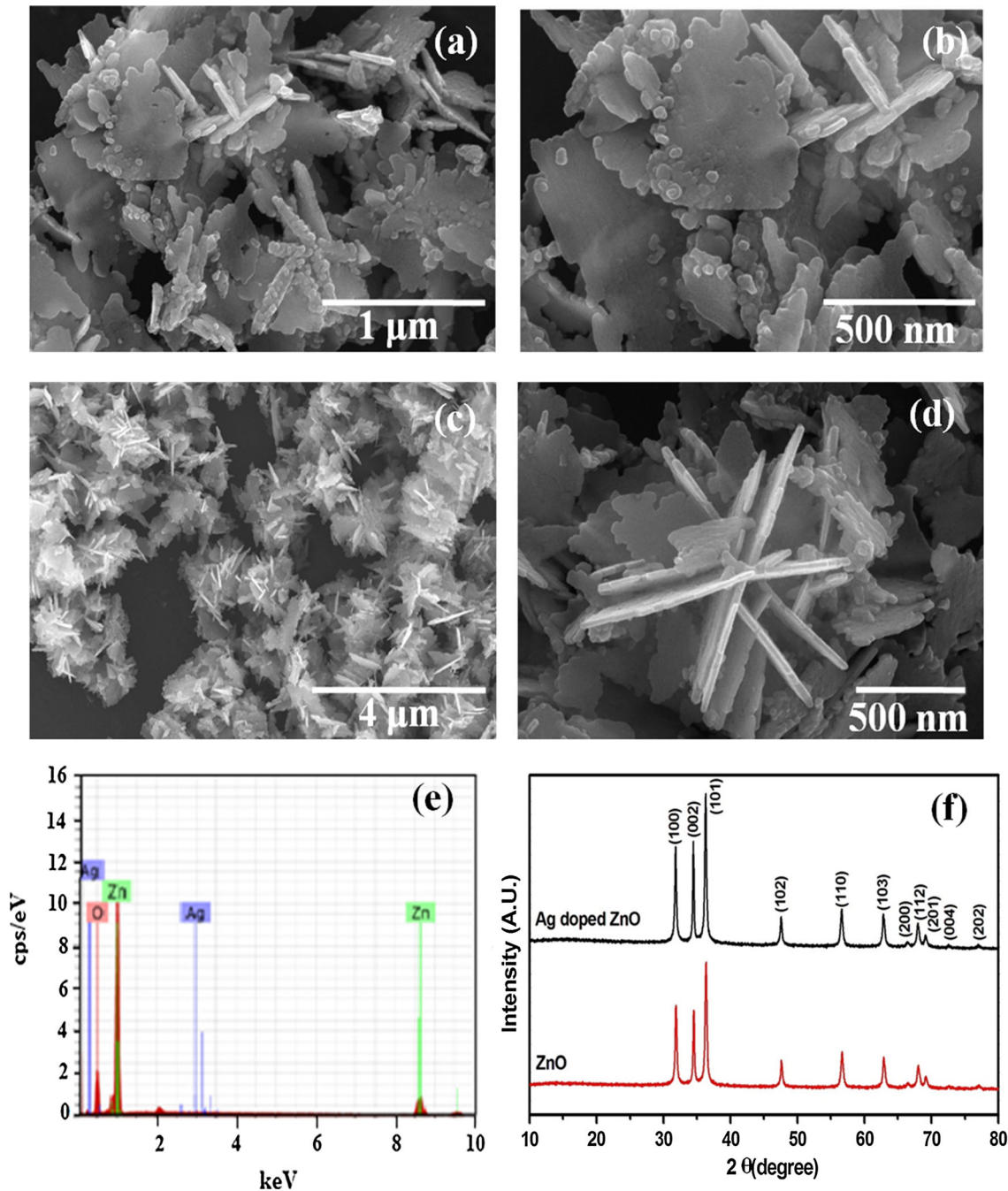


Figure 1 FESEM images **a**, **c** at low resolution, **b**, **d** at high resolution, **e** EDS and **d** XRD of Ag-doped ZnO microplates.

was measured using a UV–Vis Systronics-2202 spectrophotometer, and degradation efficiency was computed as:

$$\text{Degradation efficiency} = [1 - (C/C_0)] \times 100 \quad (1)$$

where C_0 is the initial KTC concentration, and C is KTC concentration after irradiating with solar light at a certain time.

Results and discussion

Characterization of Ag-doped ZnO powder

The morphology of Ag-doped ZnO was observed using field emission scanning electron microscope (FESEM), and typical electron micrographs are shown in Fig. 1. As seen from Fig. 1a–d, the prepared

sample consists of 2-D plate-like morphology and grown in high density. Figure 1b and d exhibits the high-resolution images which verified that microplates are formed by accretion of hundreds of nanoparticles. The typical thickness of plates is 40–50 nm, and sizes are in the range of micrometers. EDS spectrum (Fig. 1e) of Ag-doped ZnO identifies the existence of Ag in synthesized sample. XRD pattern of as-prepared ZnO and Ag-doped ZnO is shown in Fig. 1f. In case of ZnO, all the diffraction peaks are well matched with JCPDS data card no. 36–1451. XRD studies reveal that ZnO and Ag-doped catalysts exhibit various well-defined peaks of wurtzite hexagonal ZnO. In Fig. 1f, the diffraction peaks observed at $2\theta = 31.74^\circ, 34.47^\circ, 36.42^\circ, 47.53^\circ, 56.68^\circ, 62.88^\circ, 66.43^\circ, 67.92^\circ, 69.18^\circ, 72.60^\circ$ and 77.19° can be related to the crystal planes of (100), (002), (101), (102), (110), (103), (200), (112), (201), (004) and (202), respectively [23, 24]. The peak corresponding to (101) is more intense than other peaks and shows very small shifts towards decreasing 2θ value with Ag doping. The slight increase in intensities of all the peaks for Ag doping (0.025%) indicates improved crystallinity of ZnO [25]. No diffraction peak allied to Ag is detected that can be due to very small concentration of Ag^+ ions in sample, which confirms the replacement of Zn^{2+} by Ag^+ ions into ZnO matrix. The crystallite sizes of the prepared samples are calculated from Debye Scherer's equation.

$$D = 0.9\lambda/\beta \cos \theta \quad (2)$$

where λ is the wavelength of the X-ray light, β is the broadening of diffraction peak at FWHM, and θ is

Bragg's angle. The lattice constants ' a ' and ' c ' are estimated from following equation:

$$\frac{1}{d^2} = \frac{4}{3} \left[h^2 + hk + \frac{k^2}{a^2} \right] + \frac{l^2}{c^2} \quad (3)$$

The lattice constants for ZnO and doped ZnO are $a = 3.239 \text{ \AA}$, $c = 5.197 \text{ \AA}$ and $a = 3.251 \text{ \AA}$, $c = 5.201$, respectively. The crystallite size of pristine and doped ZnO is estimated as 38.45 nm and 34.15 nm, respectively. The values of lattice parameters are increased with the doping which is due to the inclusion of Ag^+ ions into ZnO lattice or substitution of Zn^{2+} with Ag^+ ions because of larger difference in radius of Zn^{2+} (0.074 nm) and Ag^+ (0.126 nm) ions [26].

The as-prepared products were examined in terms of their atomic and molecular vibration. The FTIR spectrum of Ag-doped ZnO sample was obtained in the range of wavenumber $400\text{--}4000 \text{ cm}^{-1}$ which followed a pattern similar to pristine ZnO and as shown in Fig. 2. The peak at 3373 cm^{-1} corresponded to the absorption of surface hydroxyl groups [27, 28]. The broad band positioned at 560 and 876 cm^{-1} is ascribed to the stretching vibrations of Zn–O [29]. It was inferred that the shift in band position could be as a result of the introduction of Ag^+ ions into ZnO matrix. From the TGA analysis, it was seen that the total weight loss (%) for Ag-doped ZnO and ZnO microplates was found to be 6.4 and 5.3%, respectively, in the range of $0\text{--}800 \text{ }^\circ\text{C}$. The initial weight loss for both samples up to $500 \text{ }^\circ\text{C}$ was due to the evaporation of physically and chemically adsorbed water molecules on the surface of microplates [30–32]. But the weight loss at higher temperature ($500\text{--}800 \text{ }^\circ\text{C}$)

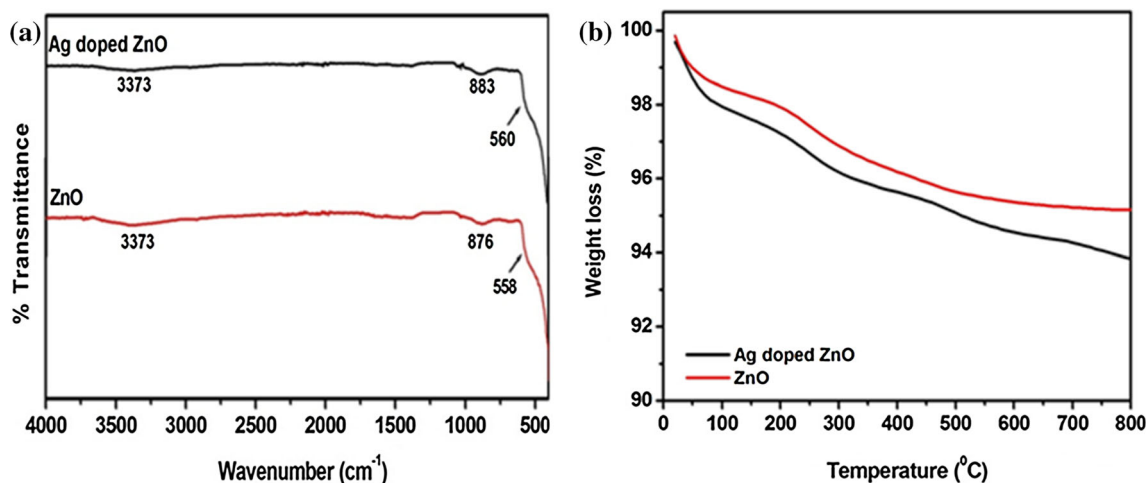


Figure 2 a FTIR spectra, b TGA of ZnO and Ag-doped ZnO microplates.

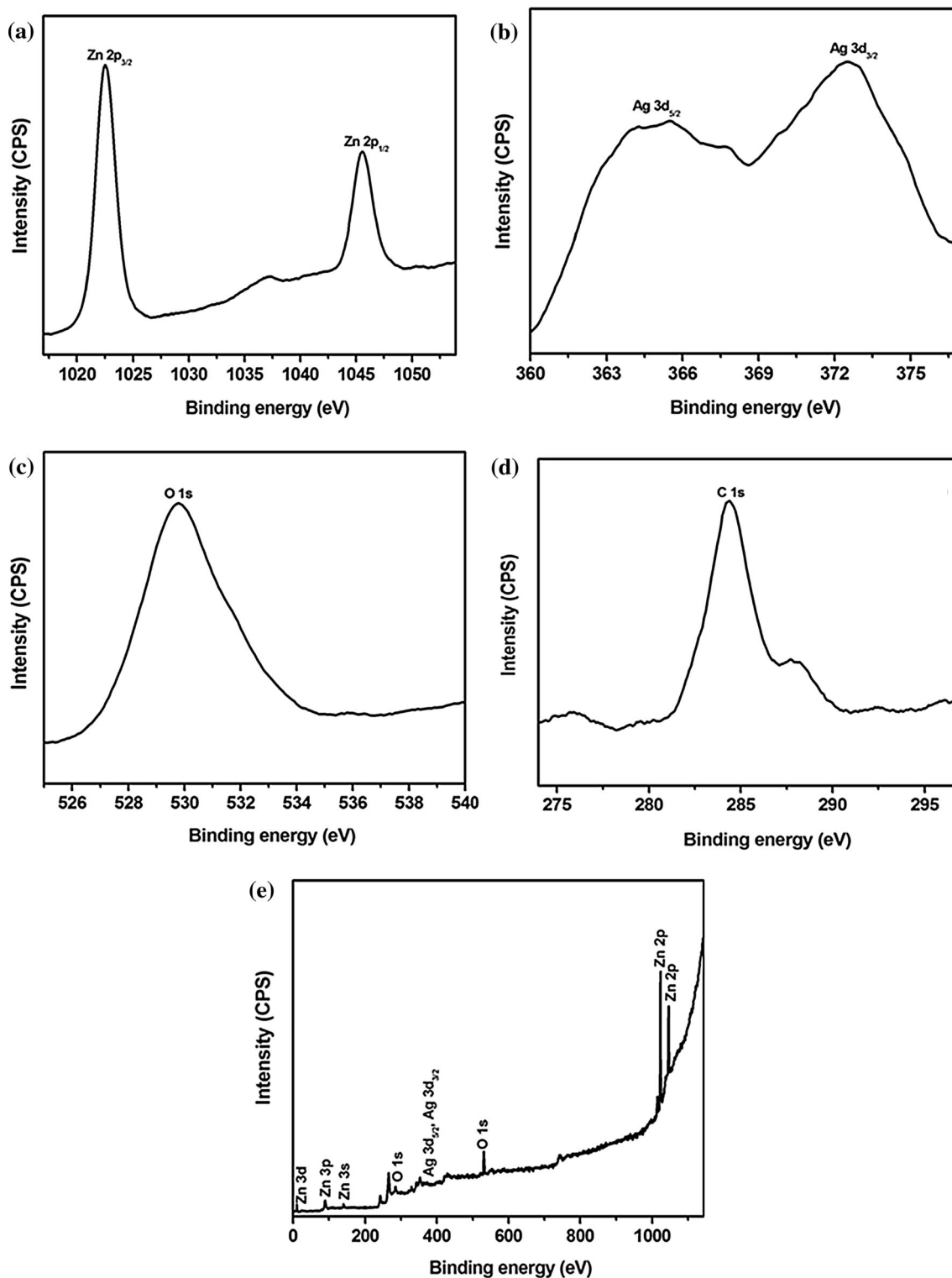


Figure 3 XPS spectra of Ag-doped ZnO microplates for **a** Zn 2p; **b** Ag 3d; **c** O 1s; **d** C 1 s and **e** full spectrum.

was about 0.5% and 1.2% for ZnO and Ag-doped ZnO, respectively, which depicts thermal stability of prepared samples.

Surface composition of the silver-doped ZnO microplates was investigated by X-ray photo electron spectroscopy. Figure 3a–e displays the scan survey

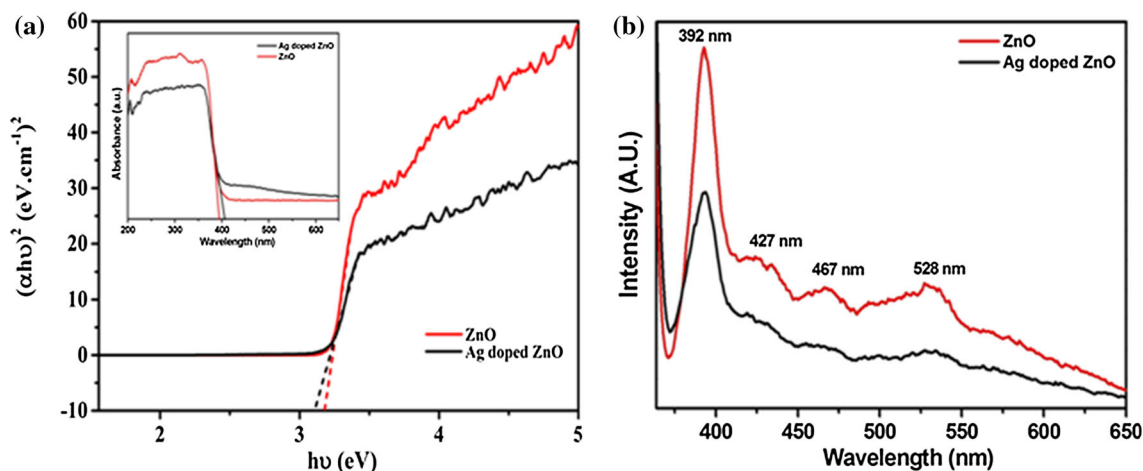


Figure 4 **a** Plot of $(\alpha hv)^2$ versus energy (hv) , (*inset*) UV–Vis DRS spectra; **b** RT-PL spectra of as-synthesized ZnO and Ag-doped ZnO microplates.

spectra of Ag-doped ZnO, and all the peaks on the curve may be corresponded to Zn, Ag, O and C element, while C 1s at 284.8 eV is because of adventitious hydrocarbon (Fig. 3d) from instrument itself. Figure 3a exhibits the Zn 2p binding energy region. The Zn $2p_{3/2}$ and $2p_{1/2}$ spin orbital states for sample are positioned at binding energy of 1023.0 eV and 1045.6 eV, respectively [33, 34]. As observed from the high-resolution Ag 3d spectrum (Fig. 3b), Ag-doped ZnO exhibited two peaks identified at 365.5 eV and 372.7 eV, corresponding to Ag $3d_{5/2}$ and Ag $3d_{3/2}$, respectively [35, 36]. These values are in agreement with metallic silver values [37, 38]. In O 1s spectrum (Fig. 3c), the peak obtained at binding energy 529.7 eV is ascribed to the lattice oxygen of ZnO. The peaks observed in the XPS spectrum overall (Fig. 3e) were in accordance with the earlier results [39].

UV–Vis DRS experiment was carried out to examine the light absorbed by the catalyst prepared. The UV–Vis spectra of the Ag-doped ZnO and ZnO catalysts are shown in inset of Fig. 4a. The synthesized Ag-doped ZnO sample showed that the absorption of light had shifted to a longer wavelength region compared to bare ZnO. A classical Tauc method was further used to estimate the energy band gap of ZnO and Ag-doped ZnO samples according to given equation [40]:

$$(\alpha hv)^n = A (hv - E_{bg}) \quad (4)$$

where α , h , v , E_{bg} and A are absorption coefficient, planck constant, light frequency, band gap and constant, respectively. Among them, n is calculated from the optical transmission of a semiconductor. The

value of n for Ag-doped ZnO and ZnO is taken as 2, because of the characteristic of direct band transition. Thus, the energy band gap of ZnO and Ag-doped ZnO can be computed from a plot of $(\alpha hv)^2$ versus hv (Fig. 4a) and was found to be 3.18 eV and 3.10 eV, respectively. Furthermore, the substitution of silver ions into Zn^{2+} sites showed red shift in band gap absorption of ZnO microplates as reported in the literature [41].

Optical properties of the prepared catalysts were monitored using RT-PL at an excitation wavelength of 340 nm, and results are shown in Fig. 4b. The PL spectrum of ZnO possesses major UV-emission peak at 392 nm and is because of the extinction of excitons, and the visible light luminescence bands centred at 427 nm and 467 nm were due to the high density of surface defects, oxygen vacancies and the recombination of free charge carriers [38]. The green emission band centred at 528 nm is because of electron–hole recombination which occupies single ion oxygen vacancy [39]. The PL intensity of Ag-doped ZnO was reduced in contrast to pristine ZnO. The PL intensity of ZnO was significantly quenched by the substitution of Ag in ZnO matrix [42], and thus Ag-doped ZnO may show higher photocatalytic activity than ZnO catalyst.

Photocatalytic performance

In order to assess the photocatalytic activity of Ag-doped ZnO microplates, various degradation experiments were performed to degrade the KTC drug under solar irradiation. Ketorolac tromethamine

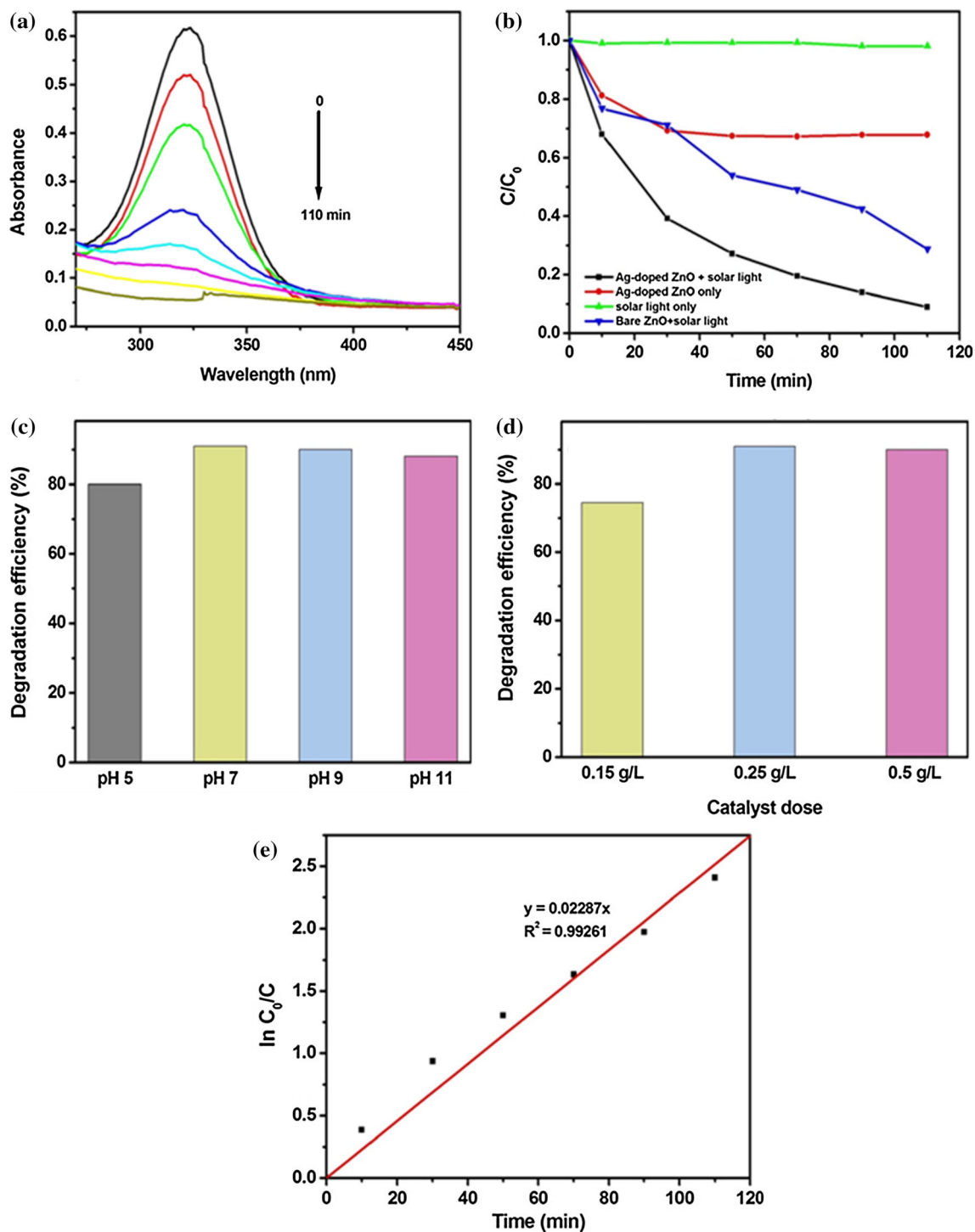


Figure 5 a UV–Vis absorbance spectra of KTC; **b** comparison of photolysis, adsorption and photocatalytic activity of bare ZnO and Ag-doped ZnO under solar light (catalyst dose 0.25 g/L, drug concentration 10 mg/L, pH 7); effect of **c** pH of drug solution;

(KTC) exhibits an absorption peak at $\lambda_{\max} = 320$ nm. Figure 5a shows photodegradation of KTC over Ag-doped ZnO microplates under solar light. It is

d catalyst dose on degradation efficiency and **e** plot of $\ln C_0/C$ versus time demonstrating photocatalytic degradation of KTC drug kinetics.

observed that the absorbance of the drug solution was reduced during the photocatalytic reactions. About 91% of KTC drug solution was degraded

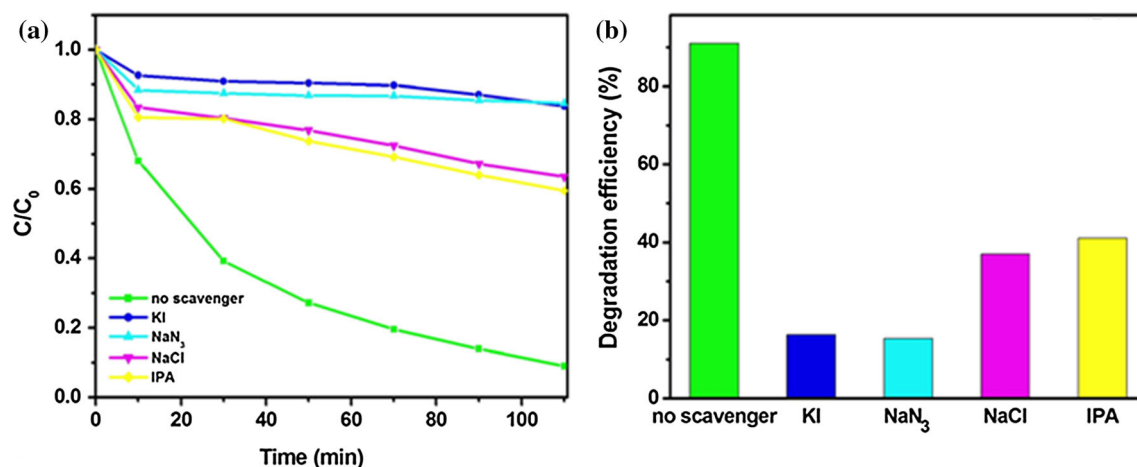


Figure 6 **a** The extent of photocatalytic degradation and **b** degradation efficiency of the KTC solution (10 mg/L) with and without different scavengers over Ag-doped ZnO microplates.

within 110 min of solar irradiation, higher than that obtained using pristine ZnO (71%) under similar conditions. It can be examined that no considerable degradation of the drug solution occurred only under solar light. However, about 32% adsorption of drug was observed on the surface of Ag-doped ZnO as shown in Fig. 5b.

The effect of initial drug pH on degradation efficiency with Ag-doped ZnO was studied by varying the pH of drug solution (10 mg/L) from 5 to 11, keeping all other conditions constant, i.e. catalyst dose (0.25 g/L). The degradation efficiency of KTC enhanced from 80% to 91%, as pH increases from 5 to 7 and achieved a maximum degradation efficiency (91%) at pH 7. On further increasing the pH from 9 to 11, degradation efficiency decreased from 90% to 88% (Fig. 5c). The photodegradation efficiency of catalyst relies on the accessibility of active sites, so it is required to optimize the catalyst dose for the degradation of drug compound.

To optimize the catalyst dose for the degradation of KTC (10 mg/L), number of experiments were performed by altering the catalyst loading from 0.15 g/L to 0.5 g/L at pH 7. It was noticed that with the increase in catalyst loading from 0.15 g/L to 0.25 g/L, the degradation efficiency of drug increased. However, as the dose was increased from 0.25 g/L to 0.5 g/L, photodegradation efficiency was decreased which could be due to the obstruction in the scattering of sunlight in hazy suspension (Fig. 5d). The photocatalytic degradation of ketorolac tromethamine using Ag-doped ZnO has not yet been described in the literature. But Ag-doped ZnO used as

photocatalyst for the degradation of other organic pollutants such as dyes and phenols [10, 43–45]. Yildirim et al. [46] studied the photocatalytic degradation of methylene orange with Ag-doped zinc oxide nanoparticles that have been reported. The authors concluded that improved photocatalytic degradation of organic pollutants including dyes was obtained with Ag-doped ZnO as compared to pristine ZnO. Complete degradation of MO dye was achieved in 90 min under UV light with 0.3% Ag-doped ZnO. Udom et al. [47] investigated the effect of Ag concentration on removal efficiency of methyl orange, and results exhibited that about 99% of methyl orange (20 mg/L) was achieved in 2 h with 1.2% Ag-doped ZnO under UV irradiation. Another study showed 99.5% degradation of methyl orange in 60 min using Ag/ZnO under simulated solar light [48]. In the present work, the prepared catalyst exhibits similar results ~91% photocatalytic activity for the degradation of KTC under solar irradiation. The reaction kinetics of ketorolac tromethamine (10 mg/L, pH 7) degradation was examined with synthesized Ag-doped ZnO (0.25 g/L), using Langmuir–Hinshelwood kinetic model [19, 28]. According to which, $\ln(C_0/C) = kt$, where C_0 is the initial concentration of drug and C is the final concentration of drug after photocatalysis at different time (t) intervals, k is the apparent rate constant and t is the degradation reaction time. Figure 5e shows the plot of $\ln(C_0/C)$ vs time for the photocatalytic degradation of KTC demonstrating conformity with pseudo first-order kinetic model with apparent reaction rate constant (k) of 0.02287 min^{-1} .

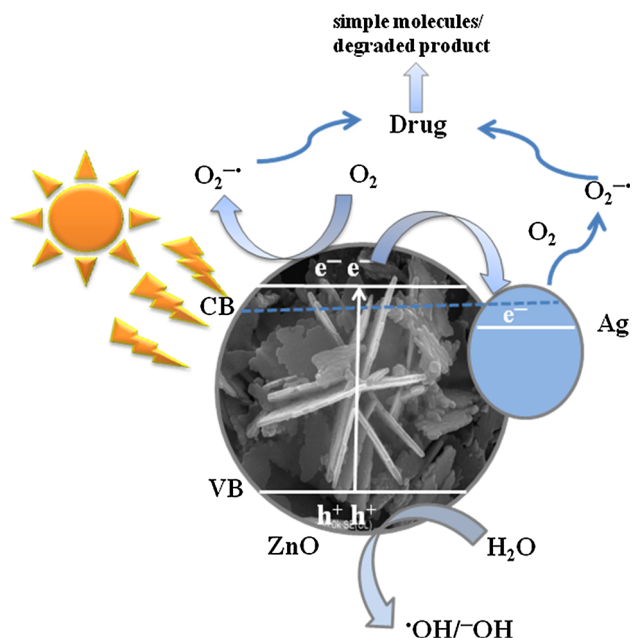


Figure 7 Photocatalytic degradation mechanism over Ag-doped ZnO microplates under solar irradiation.

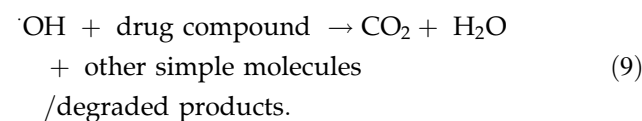
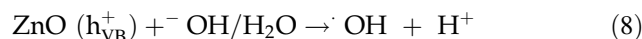
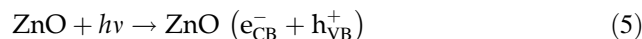
Role of primary reactive species

To determine the contribution of reactive species, various scavengers (0.01 M) were introduced into the photodegradation system prior to catalyst addition. The scavengers such as potassium iodide (KI) for h^+ and $\cdot OH_s$, sodium azide (NaN_3) for 1O_2 and $\cdot OH$, sodium chloride (NaCl) for h^+ and isopropanol (IPA) for $\cdot OH$ were employed in this study [49–51]. As shown in Fig. 6, with the addition of KI, the degradation efficiency of KTC decreased to a large extent, depicting that h^+ and $\cdot OH_s$ play important role in photocatalytic process. In addition, a major inhibition effect on the degradation performance was witnessed when NaN_3 was employed to quench 1O_2 and $\cdot OH$, verifying the significant role of reactive species in the photocatalytic degradation process. In addition, the photocatalytic degradation of KTC (91%) decreased to 37% and 41% after NaCl and IPA were added, respectively, indicating h^+ , $\cdot OH_s$, 1O_2 and $\cdot OH$ are the prime reactive species in photocatalytic degradation process.

Photocatalytic degradation mechanism

The illustrative mechanism of solar light active photocatalytic reaction on the surface of Ag-doped ZnO has been shown in Fig. 7. When light radiates the

surface of ZnO, electrons–holes are generated in the conduction and valence bands, respectively (Eq. 5). Schottky barrier is build up at the interface of ZnO and ensuing an efficient transfer of electrons from ZnO to the newly formed interface. In a doped catalyst, the excitation of electrons is effective even with lower photon energy. Meanwhile, the Ag dopant acts as an electron acceptor that traps the excited electrons from the conduction band ZnO (Eq. 6) [52], inhibits the electron–hole recombination, and thus enhances photocatalytic efficiency [53]. The photogenerated e^- react with O_2 to form O_2^- (Eq. 7). The photogenerated holes can easily be captured by $\cdot OH$ as well as H_2O to produce hydroxyl radicals ($\cdot OH$) in equation (Eq. 8). The overall photocatalytic mechanism (Eq. 9) is based on the reaction between pollutant and generated active species (O_2^- and $\cdot OH$). Ag dopant can extend the absorption of light by enhancing the photoresponse of cation loaded ZnO in the entire spectrum of solar light. However, high dopant concentration increases the recombination rate of photoexcited charge carriers and thereby decreasing the photodegradation efficiency.



Conclusions

Ag-doped ZnO microplates have been synthesized using pH-mediated precipitation technique and characterized in terms of their structural, morphological and optical properties. The as-synthesized Ag-doped ZnO microplates were employed as a potent photocatalyst, and about 91% degradation of KTC was achieved in 110 min under solar light. The Ag-doped ZnO photocatalyst also exhibited better photodegradation efficiency as compared to pristine ZnO (71%). The enhanced photocatalytic efficiency of prepared photocatalyst is due to the formation of barrier in ZnO interface and Ag dopant. Meanwhile,

Ag dopant acts as electron acceptor, and the electrons moved from conduction band of ZnO to newly formed interface and thereby decrease the $e^- + h^+$ recombination.

Acknowledgement

The authors greatly acknowledge the TEQIP-II Grant of Dr. S. S. Bhatnagar UICET, Panjab University, Chandigarh, for funding.

References

- [1] Mahvelati-Shamsabadi T, Goharshadi EK (2017) Photostability and visible-light-driven photoactivity enhancement of hierarchical ZnS nanoparticles: the role of embedment of stable defect sites on the catalyst surface with the assistant of ultrasonic waves. *Ultrason Sonochem* 34:78–89
- [2] Sood S, Umar A, Mehta SK, Kansal SK (2015) α -Bi₂O₃ nanorods: an efficient sunlight active photocatalyst for degradation of rhodamine B and 2,4,6-trichlorophenol. *Ceram Int* 41:3355–3364
- [3] Li X, Xia J, Zhu W, Di J, Wang B, Yin S, Chen Z, Li H (2016) Facile synthesis of few-layered MoS₂ modified BiOI with enhanced visible-light photocatalytic activity. *Colloids Surf A* 511:1–7
- [4] Li X, Hu Z, Liu J, Li D, Zhang X, Chen J, Fang J (2016) Ga doped ZnO photonic crystals with enhanced photocatalytic activity and its reaction mechanism. *Appl Catal B: Environ* 195:29–38
- [5] Kaur A, Kansal SK (2016) Bi₂WO₆ nanocuboids: an efficient visible light active photocatalyst for the degradation of levofloxacin drug in aqueous phase. *Chem Eng J* 302:194–203
- [6] Su J, Zhu L, Geng P, Chen G (2016) Self-assembly graphitic carbon nitride quantum dots anchored on TiO₂ nanotube arrays: an efficient heterojunction for pollutants degradation under solar light. *J Hazard Mater* 316:159–168
- [7] Ali AH, Kapoor S, Kansal SK (2011) Studies on the photocatalytic decolorization of pararosaniline chloride dye and its simulated dyebath effluent, Desalin. *Water Treat* 25:268–275
- [8] Wang Y, Li X, Lu G, Chen G, Chen Y (2008) Synthesis and photo-catalytic degradation property of nanostructured-ZnO with different morphology. *Mater Lett* 62:2359–2362
- [9] Lee KM, Lai CW, Ngai KS, Juan JC (2016) Recent developments of zinc oxide based photocatalyst in water treatment technology: a review. *Water Res* 88:428–448
- [10] Ibhaddon AO, Fitzpatrick P (2013) Heterogeneous photocatalysis: recent developments and applications. *Catalysts* 3:189–218
- [11] Subash B, Krishankumar B, Swaminathan M, Shanthi M (2013) Synthesis and characterization of cerium-silver co-doped zinc oxide as a novel sunlight-driven photocatalyst for effective degradation of reactive red 120 dye. *Mater Sci Semicond Process* 16:1070–1078
- [12] Lopes OF, Carvalho KTG, Macedo GK, de Mendonca VR, Jr WA, Rieiro C (2015) Synthesis of BiVO₄ via oxidant peroxy-method: insights into the photocatalytic performance and degradation mechanism of pollutants. *New J Chem* 39:6231–6237
- [13] Yao K, Basnet P, Sessions H, Larsen GK, Murph SEH, Zhao Y (2016) Fe₂O₃-TiO₂ core-shell nanorod arrays for visible light photocatalytic applications. *Catal Today* 270:51–58
- [14] Chong X, Zhao B, Li R, Ruan W, Yang X (2015) Photocatalytic degradation of rhodamine 6G on Ag modified TiO₂ nanotubes: surface-enhanced Raman scattering study on catalytic kinetics and substrate recyclability. *Colloids Surf A* 481:7–12
- [15] Kundu P, Deshpande PA, Madras G, Ravishankar N (2011) Nanoscale ZnO/CdS heterostructures with engineered interfaces for high photocatalytic activity under solar radiation. *J Mater Chem* 21:4209–4216
- [16] Lam S-M, Sin J-C, Abdullah AZ, Mohamed AR (2014) Transition metal oxide loaded ZnO nanorods: preparation, characterization and their UV-vis photocatalytic activities. *Sep Purif Technol* 132:378–387
- [17] Yu Q, Jiang L, Ai T (2015) Fabrication and characterization of Au-doped ZnO nanocandles synthesized on diamond film. *Mater Lett* 152:142–144
- [18] Li B, Wang Y (2011) Synthesis, microstructure, and photocatalysis of ZnO/CdS nano-heterostructure. *J Phys Chem Solids* 72:1165–1169
- [19] Chauhan R, Kumar A, Chaudhary RP (2012) Photocatalytic studies of silver doped ZnO nanoparticles synthesized by chemical precipitation method. *J Sol-Gel Sci Technol* 63:546–553
- [20] Hui A, Liu J, Ma J (2016) Synthesis and morphology-dependent antimicrobial activity of cerium doped flower-shaped ZnO crystallites under visible-light irradiation. *Colloids Surf A* 506:519–525
- [21] Yan Y, Al-Jassim MM, Wei S-H (2006) Doping of ZnO by group-IB elements. *Appl Phys Lett* 89(18):1912 (1–3)
- [22] Reddy BS, Reddy SV, Reddy NK, Kumari JP (2013) Synthesis, structural, optical properties and antibacterial activity of co-doped (Ag, Co) ZnO nanoparticles. *Res J Mater Sci* 1:11–20

- [23] Lamba R, Umar A, Mehta SK, Anderson WA, Kansal SK (2015) Visible-light-driven photocatalytic properties of self assembled cauliflower-like AgCl/ZnO hierarchical nanostructures. *J Mol Catal A: Chem* 408:189–201
- [24] Kaur A, Kansal SK (2016) Degradation of ofloxacin in aqueous phase using TiO₂/ZnO. *J Nanosci Nanotechnol - Asia* 6:113–118
- [25] Khan F, Baek S-H, Kim JH (2016) Enhanced charge transport properties of Ag and Al co-doped ZnO nanostructures via solution process. *J Alloys Compd* 682:232–237
- [26] Lupan O, Chow L, Ono LK, Cuenya BR, Chai G, Khallaf H, Park S, Schulte A (2010) Synthesis and Characterization of Ag- or Sb-doped ZnO nanorods by facile hydrothermal route. *J Phys Chem C* 114:12401–12408
- [27] Sood S, Umar A, Mehta SK, Kansal SK (2015) Highly effective Fe-doped TiO₂ nanoparticles photocatalysts for visible light driven photocatalytic degradation of toxic organic compounds. *J Colloid Interface Sci* 450:213–223
- [28] Kaur A, Umar A, Kansal SK (2015) Sunlight-driven photocatalytic degradation of non-steroidal anti-inflammatory drug based on TiO₂ quantum dots. *J Colloid Interface Sci* 459:257–263
- [29] Lamba R, Umar A, Mehta SK, Kansal SK (2015) Sb₂O₃-ZnO nanospindles: a potential material for photocatalytic and sensing applications. *Ceram Int* 41:5419–5438
- [30] Raza W, Haque MM, Muneer M (2014) Synthesis of visible light driven ZnO: characterization and photocatalytic performance. *Appl Surface Sci* 322:215–224
- [31] Barick KC, Aslam M, Dravid VP, Bahadur D (2008) Self-aggregation and assembly of size-tunable transition metal doped ZnO nanocrystals. *J Phys Chem C* 112:15163–15170
- [32] Murugadoss G (2012) Synthesis and characterization of transition metals doped ZnO nanorods. *J Mater Sci Technol* 28:587–593
- [33] Han Z, Ren L, Cui Z, Chen C, Pan H, Chen J (2012) Ag/ZnO flower heterostructures as a visible-light driven photocatalyst via surface plasmon resonance. *Appl Catal B: Environ* 126:298–305
- [34] Shi L, Liang L, Ma J, Meng Y, Zhong S, Wang F, Sun J (2014) Highly efficient visible light-driven Ag/AgBr/ZnO composite photocatalyst for degrading rhodamine B. *Ceram Int* 40:3495–3502
- [35] Ye L, Liu J, Gong C, Tian L, Peng T, Zan L (2012) Two different roles of metallic Ag on Ag/AgX/BiOX (X = Cl, Br) Visible light photocatalysts: surface plasmon resonance and Z-scheme bridge. *ACS Catal* 2:1677–1683
- [36] Carvalho P, Sampaio P, Azevedo S, Vaz C, Espinos JP, Teixeira V, Carneiro JO (2014) Influence of thickness and coating morphology in the antimicrobial performance of zinc oxide coatings. *Appl Surface Sci* 307:548–557
- [37] Ravishankar TN, Manjunatha K, Ramakrishna T, Nagaraju G, Kumar D, Sarakar S, Anandkumar BS, Chandrappa GT, Reddy V, Dupont J (2014) Comparison of the photocatalytic degradation of trypan blue by undoped and silver-doped zinc oxide nanoparticles. *Mater Sci Semicond Process* 26:7–17
- [38] Sumesh E, Bootharaju MS, Anshup T Pradeep (2011) A practical silver nanoparticle-based adsorbent for the removal of Hg²⁺ from water. *J Hazard Mater* 189:450–457
- [39] Georgekutty R, Serry MK, Pillai SC (2008) A highly efficient Ag-ZnO photocatalyst: synthesis, properties and mechanism. *J Phys Chem C* 112:13563–13570
- [40] Kumar S, Singh V, Tanwar A (2016) Structural, morphological, optical and photocatalytic properties of Ag-doped ZnO nanoparticles. *J Mater Sci: Mater Electron* 27:2166–2173
- [41] Jeong SH, Park BN, Lee SB, Boo JH (2007) Metal-doped ZnO thin films: synthesis and characterizations. *Surf Coat Technol* 201:5318–5322
- [42] Liqiang J, Yichun Q, Baiqi W, Shudan L, Baojiang J, Libin Y, Wei F, Honggang F, Jiazhong S (2006) Review on photoluminescence performance of nanosized semiconductor materials and its relationships with photocatalytic activity. *Sol Energy Mater Sol Cells* 90:1773–1787
- [43] Arsana P, Bubpa C, Sang-aroon W (2012) Photocatalytic activity under solar irradiation of silver and copper doped zinc oxide: photodeposition versus liquid impregnation methods. *J. Appl. Sci* 12:1809–1816
- [44] Behnadjady MA, Modirshahla N, Shokri M, Zeininezhad A, Zamani HA (2009) Enhanced photocatalytic activity of ZnO nanoparticles by silver doping with optimization of photodeposition method parameters. *J Environ Sci Health, Part A* 44:666–672
- [45] Wang R, Xin JH, Yang Y, Liu H, Xu L, Hu J (2004) The characteristics and photocatalytic activities of silver doped ZnO nanocrystallites. *Appl Surface Sci* 227:312–317
- [46] Yildirim OA, Unalan HE, Durucan C (2013) Highly efficient room temperature synthesis of silver doped zinc oxide (ZnO:Ag) nanoparticles: structural, optical and photocatalytic properties. *J Am Ceram Soc* 96:766–773
- [47] Udom I, Zhang Y, Ram MK, Stefanakos EK, Hepp AF, Elzein R, Schlaf R, Goswami DY (2014) A simple photolytic reactor employing Ag-doped ZnO nanowires for water purification. *Thin Solid Films* 564:258–263
- [48] Peng F, Zhu H, Wang H, Yu H (2007) Preparation of Ag-sensitized ZnO and its photocatalytic performance under simulated solar light. *Korean J Chem Eng* 24:1022–1026
- [49] Rodriguez EM, Marquez G, Tena M, Alvarez PM, Beltran FJ (2015) Determination of main species involved in the first steps of TiO₂ photocatalytic degradation of organics with the

- use of scavengers: the case of ofloxacin. *Appl Catal B: Environ* 178:44–53
- [50] Xiao X, Hu R, Liu C, Xing C, Qian C, Zuo X, Nan J, Wang L (2013) Facile large-scale synthesis of β - Bi_2O_3 nanospheres as a highly efficient photocatalyst for the degradation of acetaminophen under visible light irradiation. *Appl Catal B: Environ* 140–141:433–443
- [51] Wang X, Tang Y, Chen Z, Lim T-T (2012) Highly stable heterostructured Ag-AgBr/ TiO_2 composite: a bifunctional visible-light active photocatalyst for destruction of ibuprofen and bacteria. *J Mater Chem* 22:23149–23158
- [52] Paul KK, Ghosh R, Giri PK (2016) Mechanism of strong visible light photocatalysis by Ag_2O -nanoparticle decorated monoclinic TiO_2 (B) porous nanorods. *Nanotechnology* 27:315703
- [53] Zhang D (2011) Photocatalytic oxidation of organic dyes with nanostructured zinc dioxide modified with silver metals. *Russ J Phys Chem* 85:1416–1422